

Synthesis of Core@shell Structured CuFeS₂@TiO₂ Magnetic Nanomaterial and Its Application for Hydrogen Production by Methanol Aqueous Solution Photosplitting

Sora Kang, Byeong Sub Kwak, Minkyu Park, Kyung Mi Jeong,[†] Sun-Min Park,[‡] and Misook Kang*

Department of Chemistry, College of Science, Yeungnam University, Gyeongsan 712-749, Korea

*E-mail: mskang@ynu.ac.kr

[†]Department of Engineering in Energy and Applied Chemistry, Silla University, Busan 617-736, Korea

[‡]Korean Institutes of Ceramic Engineering and Technology (KICET), Seoul 153-801, Korea

Received April 10, 2014, Accepted May 29, 2014

A new magnetic semiconductor material was synthesized to enable separation after a liquid-type photocatalysis process. Core@shell-structured CuFeS₂@TiO₂ magnetic nanoparticles were prepared by a combination of solvothermal and wet-impregnation methods for photocatalysis applications. The materials obtained were characterized using X-ray diffraction, transmission electron microscopy, ultraviolet-visible, photoluminescence spectroscopy, Brunauer-Emmett-Teller surface area measurements, and cyclic voltammetry. This study confirmed that the light absorption of CuFeS₂ was shifted significantly to the visible wavelength compared to pure TiO₂. Moreover, the resulting hydrogen production from the photo-splitting methanol/water solution after 10 hours was more than 4 times on the core@shell structured CuFeS₂@TiO₂ nanocatalyst than on either pure TiO₂ or CuFeS₂.

Key Words : Core@shell structure, CuFeS₂@TiO₂, Magnetic property, Methanol/water splitting, Hydrogen production

Introduction

The use of hydrogen as an energy source is expected to increase because of its environmentally friendly nature. Of the methods for generating hydrogen, the photocatalytic splitting of water using TiO₂^{1,2} and MTiO₃^{3,4} semiconductors has attracted considerable attention. The principle of photocatalytic water splitting is based on the conversion of light energy to electricity upon the exposure of a semiconductor to light. Upon exposure to incident light, the electrons of *n*-type semiconducting materials are emitted from the conduction band to the valence bands, leading to the holes in valence bands. These electrons and holes split water molecules into oxygen and hydrogen.⁵ The band gap required for hydrogen production by water splitting needs to be at least 1.2 eV. Pure TiO₂ and various MTiO₃ photocatalysts (where M = a metal) have band gaps of 3.0-5.0 eV, making them ineffective in this reaction. In addition, hydrogen production is limited by the rapid recombination of holes and electrons.⁶ To overcome this rapid recombination, considerable efforts have been made to increase hydrogen evolution using methanol, ethanol, or a mixture of light alcohol and water, rather than water because lower energies of approximately 0.6-0.8 eV are needed.^{7,8}

One issue in a liquid photocatalytic reaction is how to recover the catalyst from a liquid solution after the reaction. This paper introduces a core@shell multi-component catalyst, which has attracted considerable attention recently because of its potential applications in electronics, magnetism, optics,

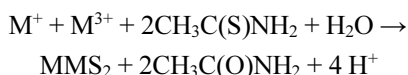
and catalysis.⁹⁻¹³ The magnetic core used can be collected conveniently and separated using a magnet. Therefore, magnetic-based TiO₂ photocatalyst synthesis will be very useful. On the other hand, it is difficult to produce TiO₂-coated particles with UV or visible-light photoactivity without sacrificing the magnetic properties. Some studies evaluated the use of magnetite (Fe₃O₄) cores.¹⁴⁻¹⁷ Recently, more stable transition-metal incorporated MFe₂O₄ (M = Ni, Co, Fe, Sr) super-paramagnetic materials have been used as core materials and have produced good results for the photocatalytic destruction of organic compounds.¹⁸⁻²¹ On the other hand, oxygenated cores are difficult to activate under visible-light, so materials containing sulfur or nitrogen are used. Therefore, the perfect core@shell structured MFeS₂@TiO₂ magnetic photocatalysts require further development. Furthermore, higher photocatalytic activity can be expected when a metal with higher reduction potentials, Cu or Ag, is inserted into MFeS₂ core, but comparatively little developmental work has been conducted on redox applications.

The major objective of this study was to develop core@shell-structured CuFeS₂@TiO₂ photocatalysts with improved catalytic properties for the production of hydrogen from methanol/water aqueous systems, and with magnetic properties commensurate with the separations. The nature of the CuFeS₂@TiO₂ photocatalyst produced was examined by X-ray diffraction (XRD), UV-visible spectroscopy, photoluminescence (PL) spectroscopy, Brunauer-Emmett-Teller (BET) surface area measurements, and magnetic momentum using a vibrating sample magnetometer.

Experimental

Core@shell structured $\text{CuFeS}_2@\text{TiO}_2$ was prepared using sequential solvothermal and impregnation hybrid methods, as shown in Figure 1. In step 1 of a), to prepare the CuFeS_2 sol mixture, iron chloride ($\text{FeCl}_3 \cdot 6\text{H}_2\text{O}$, 99.95%, Junsei Chemical, Japan) and copper chloride ($\text{CuCl}_2 \cdot 2\text{H}_2\text{O}$, 99.95%, Junsei Chemical, Japan) were used as the Fe and Cu precursors, respectively, and ethanol was used as the solvent. Briefly, 0.04 mol of FeCl_3 and 0.04 mol of CuCl_2 were added to 400 mL of ethanol, and stirred for 1 h.

Thioacetamide ($\text{C}_2\text{H}_5\text{NS}$) was added to the upper solution as a sulfur source. Thioacetamide is used widely in classical qualitative inorganic analysis as an in situ source of sulfide ions. Therefore, the treatment of aqueous solutions of many metal cations to a solution of thioacetamide affords the corresponding metal sulfide:



In the next step, ethylenediamine was added to reduce Fe^{3+} to $\text{Fe}^{2.5+}$. The final solution was stirred until it became homogeneous, and was then treated thermally in an autoclave at 200 °C for 2 h. After the thermal treatment, the obtained powder was cooled, washed with ethanol, and dried at 80 °C for 24 h. Here, pure TiO_2 was also synthesized using a solvothermal method, which is the same process (b) to CuFeS_2 .²² Titanium tetraisopropoxide (TTIP, Junsei Chemical, Japan) was used as the Ti precursor. The solution in the synthesis step was fixed to pH = 3, and the thermal treatment was performed in an autoclave at 200 °C for 8 h. In step 3 of c), the magnetic CuFeS_2 particles were coated with TiO_2 . The CuFeS_2 and TiO_2 with a 1.0 molar ratio were added to 100 mL of ethanol and its pH was fixed to 5 by HCl. The resulting colloid was stirred for 3 h. After stirring the solution until it became homogeneous, the colloid was evaporated at 70 °C for 3 h. The resulting precipitate was heated to 200 °C for 2 h under argon to remove the solvent and generate an anatase shell.

The TiO_2 , CuFeS_2 , and $\text{CuFeS}_2@\text{TiO}_2$ (analyzed as

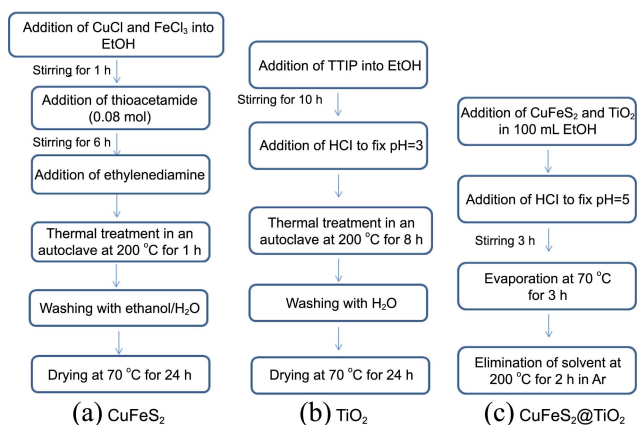


Figure 1. Synthetic sequence for the TiO_2 , CuFeS_2 , and $\text{CuFeS}_2@\text{TiO}_2$ photocatalyst.

approximately $\text{CuFeS}_2:\text{TiO}_2 = 1:1$) powders were examined by XRD (X'Pert Pro MPD PANalytical 2-circle diffractometer) using nickel-filtered $\text{CuK}\alpha$ radiation (30 kV, 30 mA) at 2θ angles from 5 to 70°, a scan speed of 10° min^{-1} , and a time constant of 1 s. The sizes and shapes of the TiO_2 , CuFeS_2 , and $1\text{CuFeS}_2@1\text{TiO}_2$ particles were determined by transmission electron microscopy (TEM, JEOL 2000EX) at 200 kV. The specific surface area and pore size distribution were calculated according to the BET theory, which gives the isotherm equation for multilayer adsorption by the generalization of Langmuir's treatment of a multi-molecular layer. The adsorption-desorption isotherm analysis to identify the BET surface area and pore size distribution of particles was performed using a Belsorp II instrument. All the particles were degassed under vacuum at 150 °C for 2 h before the measurements, and measured by nitrogen gas adsorption using a continuous flow method with a mixture of nitrogen and helium as the carrier gas. The UV-visible spectra of the TiO_2 , CuFeS_2 , and $1\text{CuFeS}_2@1\text{TiO}_2$ powders were obtained using a Shimadzu MPS-2000 spectrometer (Kyoto, Japan) equipped with a reflectance sphere over the range, 200 to 800 nm. The magnetic properties were measured using a vibrating sample magnetometer (VSM) on a physical property measurement system (Quantum Design PPMS-9). Photoluminescence (PL) spectroscopy was carried out on the three powders to examine photo-excited electron hole pairs using 1.0 mm thick pellets of TiO_2 , CuFeS_2 , and $1\text{CuFeS}_2@1\text{TiO}_2$ at room temperature using a He-Cd laser source at a wavelength of 325 nm.

The photosplitting of methanol/water was performed using a liquid photo reactor designed in this laboratory.²³ To photosplit methanol/water (1:1 vol./vol., total volume = 1.0 L) solution, 0.5 g of powdered TiO_2 , CuFeS_2 , and $1\text{CuFeS}_2@1\text{TiO}_2$ photocatalysts were added to 1.0 L of a methanol/water solution in a 2.0-L Pyrex reactor. UV-lamps ($6 \times 3 \text{ Wcm}^{-2} = 18 \text{ Wcm}^{-2}$, 30 cm length \times 2.0 cm diameter; Shinan, Korea) emitting at 365 nm were used. The photosplitting of methanol/water was carried out over 1-8 h with stirring, and hydrogen evolution was measured after 1 h of operation. The hydrogen gas (H_2) produced during methanol/water photosplitting was analyzed by TCD-type gas chromatography (GC; model DS 6200; Donam Instruments Inc., Korea). To identify the products and intermediates, GC was connected directly to a photo-reactor. The following GC conditions were used: TCD detector; Carbosphere column (Alltech, Deerfield, IL, USA); injection temperature 140 °C; initial temperature 120 °C; final temperature 120 °C; and detector temperature 150 °C.

Results and Discussion

Figure 2(a) and (b) shows XRD patterns and TEM images of the TiO_2 , CuFeS_2 , and $1\text{CuFeS}_2@1\text{TiO}_2$ powders. First in A), TiO_2 particles had a pure anatase structure with peaks at 25.3, 38.0, 48.2, 54, 63, and 68° 2θ , which were assigned to the (101), (004), (200), (105), (211), and (204) planes, respectively.²⁴ CuFeS_2 showed several peaks at 2θ values of 29.45 (d_{112}), 34.19° (d_{200}), 48.93° (d_{220}), 57.95° (d_{321}), 71.40°

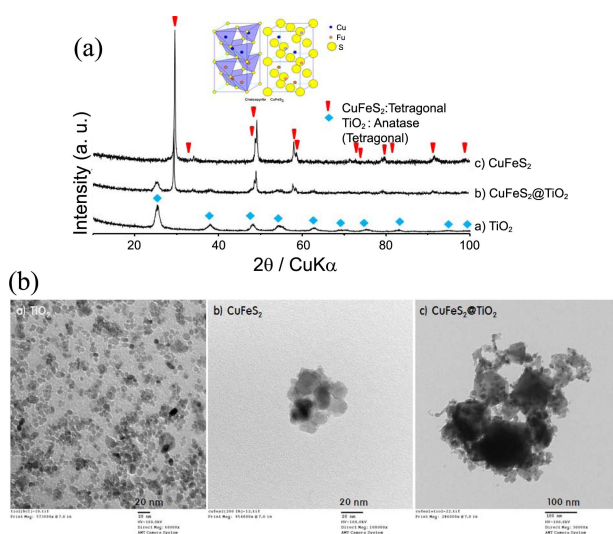
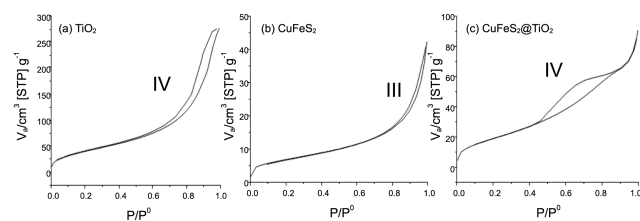


Figure 2. XRD patterns (a) and TEM photographs (b) of synthesized TiO₂, CuFeS₂, and CuFeS₂@TiO₂ powders.



Sample	BET surface area [m ² g ⁻¹]	Total pore volume [cm ³ g ⁻¹]	Average pore diameter [nm]
TiO ₂	154.21	0.43	11.14
CuFeS ₂	24.50	0.07	10.67
CuFeS ₂ @TiO ₂	73.70	0.1	7.44

Figure 3. Adsorption-desorption isotherm curves of N₂ at 77 K for the TiO₂, CuFeS₂, and 1CuFeS₂@1TiO₂ powders.

(d₄₀₀), 79.07° (d₃₃₂), and 90.99° (d₄₁₅), indicating a tetragonal crystal system (I-42d).²⁵ 1CuFeS₂@1TiO₂ showed a mixed peaks of CuFeS₂ and TiO₂, indicating the exposed CuFeS₂ or partially-covered TiO₂ on the surfaces of CuFeS₂ particles. On the other hand, peak broadening indicates a reduction in the crystallite size.²⁶ The Debye-Scherrer's equation, $t = 0.9\lambda/\beta\cos\theta$ (where λ is the wavelength of incident X-rays, β is the full width at half maximum height in radians, and the θ is the diffraction angle) was used to determine the crystallite size.²⁷ The calculated values at the representative 101 and 112 planes of TiO₂ and CuFeS₂ were 7.3 nm and 38.38 nm, respectively. The TEM images in Figure 2(b) showed slightly distorted tetragonal CuFeS₂ particles, 20 nm in size. The 1CuFeS₂@1TiO₂ particles were partially covered by 5-10 nm TiO₂ particles, and the particle size increased to 100 nm after core@shell formation compared to the size of pure CuFeS₂.

Figure 3 shows the adsorption-desorption isotherm curves of N₂ at 77 K for the TiO₂, CuFeS₂, and 1CuFeS₂@1TiO₂ powders. The isotherms of TiO₂ and 1CuFeS₂@1TiO₂ belonged to IV type in the IUPAC classification²⁸; this hysteresis slope has been observed in the presence of

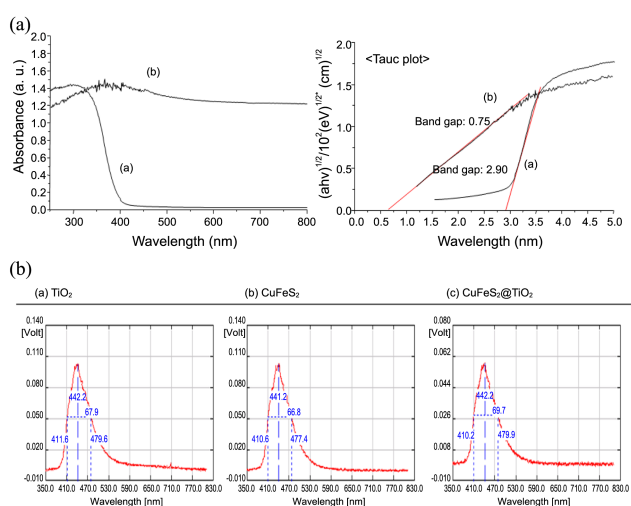


Figure 4. UV-visible diffuse reflectance spectra (a) and photoluminescence (PL) (b) spectra of TiO₂, CuFeS₂, and CuFeS₂@TiO₂ powders.

mesopores. The mesopores are considered to be bulk pores formed between the TiO₂ particles. Otherwise, the isotherms of CuFeS₂ mean non-pores with an III type. This suggests that a high surface area facilitates adsorption, which can generate adsorption activity. Therefore, some molecules are adsorbed more easily on the surfaces of the TiO₂ and core@shell structured 1CuS@1TiO₂ than CuFeS₂. On the other hand, the surface area, pore volume, and pore size are listed in the table below. The specific surface areas of TiO₂ and 1CuFeS₂@1TiO₂ were large, 154.21 and 73.70 m²g⁻¹, respectively. On the other hand, it decreased in CuFeS₂ to 24.50 m²g⁻¹. Here, the specific surface area in this study might depend on the bulk pores formed by aggregation between the TiO₂ particles in the shell, and the pore volumes showed the same tendency to the surface areas.

The UV-visible diffuse reflectance (a) and PL spectra (b) of TiO₂ and CuFeS₂ powders were also obtained (Figure 4). The absorption band corresponding to the octahedral symmetry of Ti⁴⁺ was observed at ~350 to 380 nm, indicating a band-gap of 2.90 eV.²⁹ Generally, the band gaps of semiconductor materials are closely related to the absorption wavelength, where a higher wavelength indicates a smaller band gap. CuFeS₂ exhibited a continuous absorption band in the range 200-700 nm, which concurs with its black color. Using Tauc's equation,³⁰ its band-gap was estimated to be approximately 0.75 eV. Figure 4(b) presents the photoluminescence (PL) spectra of TiO₂, CuFeS₂, and 1CuFeS₂@1TiO₂ pellets. The PL emission spectra are useful for examining the efficiency of the charge transfer behavior of photo-generated electrons and holes. The PL curves show that the electrons in the valence band are transferred to the conduction band, and then return to the valence band by photoemission. In general, the PL intensity increases with increasing number of photons emitted as a result of the recombination of electrons and holes, resulting in a decrease in photoactivity.³¹ Therefore, there is a strong relationship between the PL intensity and photoactivity. The PL spectrum of 1CuFeS₂@1TiO₂ showed

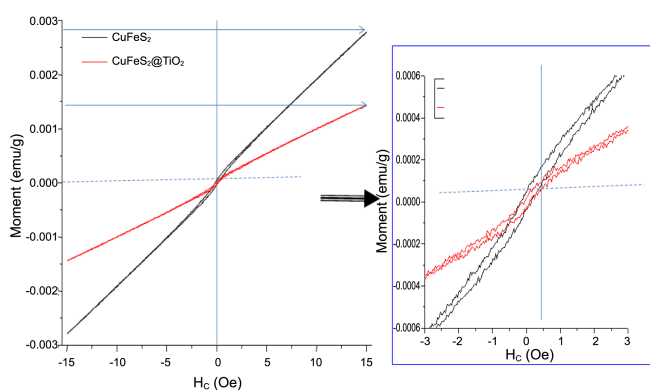


Figure 5. Saturation magnetization (M) versus coercivity (H_c) plots obtained at room temperature for CuFeS_2 and $\text{CuFeS}_2@$ TiO_2 .

that the PL intensity of TiO_2 was quenched substantially by the CuFeS_2 magnetic core. The CuFeS_2 in $1\text{CuFeS}_2@1\text{TiO}_2$ captures photo-generated electrons from the TiO_2 conduction band, in particular Cu ions, which separates the photo-generated electron-hole pairs. The presence of Cu in the CuFeS_2 magnetic core reduces the recombination rate, and reduces the PL spectrum intensity, indicating that the PL intensity depends on electron capture by Cu ions.

Figure 5 shows the saturation magnetization (emu/g) versus coercivity (H_c) plots obtained at room temperature for CuFeS_2 and $\text{CuFeS}_2@$ TiO_2 , and the inset shows an enlarged figure at an almost zero applied magnetic field. The two samples have hysteresis cycles that are characteristic of ferromagnetism. The saturation magnetizations of CuFeS_2 and $\text{CuFeS}_2@$ TiO_2 were similar but the value of CuFeS_2 was approximately two times larger than that of $\text{CuFeS}_2@$ TiO_2 . This suggests that the TiO_2 shell was responsible for the observed reduction in ferromagnetism. The TiO_2 anatase structure is diamagnetic.^{32,33} Occasionally, some Ti^{4+} ions become Ti^{3+} ions if defects are present in the TiO_2 structure, resulting in the detection of weak ferromagnetism.³⁴ Therefore, the ferromagnetic effect of TiO_2 depends on the method of synthesis, due to the presence of defects, particularly oxygen vacancies in TiO_2 nanomaterials. In addition, an advantage of $\text{CuFeS}_2@$ TiO_2 is that it can be recovered by a magnet after the reaction.

The CV results for TiO_2 and CuFeS_2 (Figure 6) were strongly dependent on the analytical conditions used, and a semiconductor needs to be redox active within the experimental potential window. In this study, the potentials were measured in distilled water using a pelletized sample as the working electrode, Ag/AgCl as the reference electrode, and 0.1 M KCl as the supporting electrolyte. A reversible wave was observed, which gives the following information: reversible reactions display a hysteresis of the absolute potential between the reduction (E_{pc}) and oxidation (E_{pa}) peaks. Reversible reactions show the ratios of the peak voltages under reduction and oxidation conditions that are near unity ($1 = E_{pa}/E_{pc}$). When such reversible peaks are observed, the thermodynamic information in the form of half-cell potentials, $E_{1/2}^0 (E_{pc} + E_{pa}/2)$ can be determined. In particular, when the

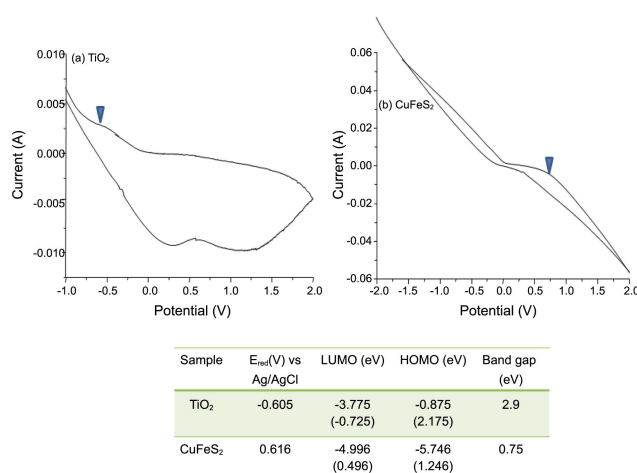


Figure 6. CV curves of TiO_2 and CuFeS_2 powders.

waves are semi-reversible, such as when E_{pa}/E_{pc} is $< \text{or} > 1$, it is possible to obtain more information on the kinetic processes. A useful equation has been reported,³⁵ which can determine the energy levels of the highest occupied molecular orbital (HOMO) and the lowest unoccupied molecular orbital (LUMO) using CV. First, the ferrocene ($E_{1/2}$ vs. $\text{Ag}/\text{Ag}^+ = +0.42$ eV) potential (a standard) should be measured in an electrolyte solution using the same reference electrode with -4.8 eV fixed as an energy level. Finally, the HOMO and LUMO energy levels can be calculated using the following formula: $\text{HOMO (or LUMO) (eV)} = -4.8 - (E_{onset} - E_{1/2}(\text{Ferrocene}))$. Here, E_{onset} is the starting point of the redox potential, and is used more than peak potential values. The onset potentials for reduction with an Ag/AgCl reference electrode for TiO_2 and CuFeS_2 were -0.605 and 0.616 V respectively. The calculated LUMO energy levels for TiO_2 and CuFeS_2 were -3.775 and -4.996 eV respectively. This was attributed to TiO_2 electrons in the valence bands absorbing solar radiation and being excited to the conduction band. These excited electrons then move in the conduction bands to CuFeS_2 . $\text{CuFeS}_2@$ TiO_2 exhibited more oxidation-reduction behavior than pure TiO_2 or CuFeS_2 . Therefore, the relaxation of excited electrons is difficult, which reduces hole/electron recombination.

The evolutions of H_2 from the photo-splitting of methanol/water over TiO_2 , CuFeS_2 , and $\text{CuFeS}_2@$ TiO_2 powders at various molar ratios were measured in a batch-type liquid photo system and are presented in Figure 7. No H_2 was collected from the photodecomposition of methanol/water over pure anatase CuFeS_2 after 10 h, whereas 1.80 mmol of H_2 was collected over $1\text{CuFeS}_2@0.05\text{TiO}_2$. This was attributed to excited electron capture by the CuFeS_2 core and a reduced recombination rate. Otherwise, evolved oxygen and carbon dioxide gases could not be observed because they were partially transformed into some by-products, such as formaldehyde, acetaldehyde, formic acid, and acetic acid, by oxidation reactions with methanol molecules. On the other hand, the expected mechanism of charge separation and the photocatalytic process of CuFeS_2 and TiO_2 are

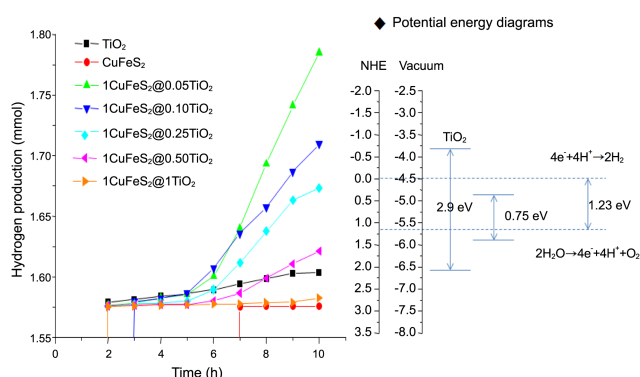


Figure 7. Evolution of H₂ from the photo-splitting of methanol/water over TiO₂, CuFeS₂ and CuFeS₂@TiO₂ powders along with the expected mechanism of charge separation and the photocatalytic process of CuFeS₂@TiO₂.

shown in the adjoining diagram based on the UV-visible and CV spectra results. The conduction band position in the CuFeS₂ core is at a lower energy than that in the TiO₂ shell. Therefore, the core could act as a sink for photo-generated electrons. Under UV-light irradiation, the excited electrons from the valence band of the TiO₂ shell move into its conduction band and flowed to the surface of the shell, and they fell into the conduction band of the CuFeS₂ magnetic core. XPS confirmed that the Cu ions in CuFeS₂ were reduced after the photoreaction, meaning that the core attracts electrons during the photoreaction. Therefore, Cu⁺ ions (3d⁹) can accept electrons, and the electrons that move from the TiO₂ shell into CuFeS₂ core can be located in the 3d orbital of Cu ions.

Conclusion

Core@shell-structured CuFeS₂@TiO₂ was synthesized for the production of H₂ gas from the photodecomposition of methanol/water in a batch-type liquid photo system. The core@shell morphology of synthesized CuFeS₂@TiO₂ was examined by XRD and TEM. The PL intensity of CuFeS₂@TiO₂, indicating electron/hole recombination, decreased. The ferromagnetic property of CuFeS₂ was decreased slightly by the presence of a TiO₂ shell. Hydrogen production from methanol/water was remarkably higher for 1CuFeS₂@0.05TiO₂ than for pure TiO₂, and 1.80 mmol of H₂ was collected after 10 h when 0.5 gL⁻¹ of the powder was used. These results suggest that hydrogen production by methanol/water splitting can be achieved more readily over the CuFeS₂@TiO₂ magnetic material. The significant enhancement in photoactivity for methanol/water mixture splitting was attributed to the synergism between CuFeS₂ and TiO₂, *i.e.*, to effective charge transfer from TiO₂ to CuFeS₂ and the suppression of electron/hole pair recombination.

Acknowledgments. This study was supported by the National Research Foundation of Korea grant funded by the Korea government (MEST) (No. 2012R1A1A3005043), for which the authors are very grateful.

References

- Lin, Y. C.; Liu, S. H.; Syu, H. R.; Ho, T. H. *Spectrochim. Acta A Mol. Biomol. Spectrosc.* **2012**, *95*, 300.
- Liu, S. H.; Syu, H. R. *Appl. Energy* **2012**, *100*, 148.
- Khemthong, P.; Photai, P.; Grisdanurak, N. *Int. J. Hydrogen Energy* **2013**, *38*, 15992.
- Jin, Z.; Zhang, X.; Li, Y.; Li, S.; Lu, G. *Catal. Commun.* **2007**, *8*, 1267.
- Zoua, Z.; Ye, J.; Arakawa, H. *Int. J. Hydrogen Energy* **2003**, *28*, 663.
- Mizoguchi, H.; Ueda, K.; Orita, M.; Moon, S. C.; Kajihara, K.; Hirano, M.; Hosono, H. *Mater. Res. Bull.* **2002**, *37*, 2401.
- Kandiel, T. A.; Dillert, R.; Robben, L.; Bahnemann, D. W. *Catal. Today* **2011**, *161*, 196.
- Ruiza, S. O.; Zanella, R.; Lópezb, R.; Gordillo, A. H.; Gómez, R. *J. Hazard. Mater.* **2013**, *263*, 2.
- Fu, W.; Yang, H.; Li, M.; Chang, L.; Yu, Q.; Xu, J.; Zou, G. *Mater. Lett.* **2006**, *60*, 2723.
- Li, C. J.; Wang, J. N.; Wang, B.; Gong, J. R.; Lin, Z. *Mater. Res. Bull.* **2012**, *47*, 333.
- Wilson, A.; Mishra, S. R.; Gupta, R.; Ghosh, K. *J. Magn. Magn. Mater.* **2012**, *324*, 2597.
- Liang, H.; Niu, H.; Li, P.; Tao, Z.; Mao, C.; Song, J.; Zhang, S. *Mater. Res. Bull.* **2013**, *48*, 2415.
- Amarjargal, A.; Tijing, L. D.; Im, I. T.; Kim, C. S. *Chem. Eng. J.* **2013**, *226*, 243.
- Xin, T.; Ma, M.; Zhang, H.; Gu, J.; Wang, S.; Liu, M.; Zhang, Q. *Appl. Surf. Sci.* **2014**, *288*, 51.
- Wu, S. H.; Wu, J. L.; Jia, S. Y.; Chang, Q. W.; Ren, H. T.; Liu, Y. *Appl. Surf. Sci.* **2013**, *287*, 389.
- Chi, Y.; Yuan, Q.; Li, Y.; Zhao, L.; Li, N.; Li, X.; Yand, W. *J. Hazard. Mater.* **2013**, *262*, 404.
- Ma, P.; Jiang, W.; Wang, F.; Li, F.; Shen, P.; Chen, M.; Wang, Y.; Liu, J.; Li, P. *J. Alloys Compd.* **2013**, *578*, 501.
- Mohapatra, S.; Rout, S. R.; Panda, A. B. *Colloids Surf., A: Physicochem. Eng. Aspects* **2011**, *384*, 453.
- Wang, L.; Li, J.; Wang, Y.; Zhao, L.; Jiang, Q. *Chem. Eng. J.* **2012**, *181-182*, 72.
- Goyal, A.; Bansal, S.; Singha, S. *Int. J. Hydrogen Energy* **2014**, *39*, 4895.
- Xiong, P.; Fu, Y.; Wang, L.; Wang, X. *Chem. Eng. J.* **2012**, *195-196*, 149.
- Lee, Y.; Chae, J.; Kang, M. *J. Ind. Eng. Chem.* **2010**, *16*, 609.
- Kim, H. S.; Kim, D.; Kwak, B. S.; Han, G. B.; Um, M. H.; Kang, M. *Chem. Eng. J.* **2014**, *243*, 272.
- Lee, G.; Kang, M. *Curr. Appl. Phys.* **2013**, *13*, 1482.
- Wang, Y. H. A.; Bao, N.; Gupta, A. *Solid State Sci.* **2010**, *12*, 387.
- Liu, H.; Wang, M.; Wang, Y.; Liang, Y.; Cao, W.; Su, Y. *J. Photochem. Photobiol., A: Chem.* **2011**, *223*, 157.
- Leong, K. H.; Monash, P.; Ibrahim, S.; Saravanan, P. *Sol. Energy* **2014**, *101*, 321.
- Rashad, M. M.; Elsayed, E. M.; Al-Kotb, M. S.; Shalan, A. E. *J. Alloys Compd.* **2013**, *581*, 71.
- Kim, J.; Kang, M. *Int. J. Hydrogen Energy* **2012**, *37*, 8249.
- Dua, J.; Chen, H.; Yang, H.; Sang, R.; Qian, Y.; Li, Y.; Zhu, G.; Mao, Y.; He, W.; Kang, D. *J. Microporous Mesoporous Mater.* **2013**, *182*, 87.
- Zhang, W.; Zhao, J.; Liu, Z.; Liu, Z.; Fu, Z. *Appl. Surf. Sci.* **2010**, *256*, 4423.
- Lyubutin, I. S.; Lin, C. R.; Starchikov, S. S.; Siao, Y. J.; Shaikh, M. O.; Funtov, K. O.; Wang, S. C. *Acta Mater.* **2013**, *61*, 3956.
- Fan, L.; Dongmei, J.; Yan, L.; Xueming, M. *Phys. B: Condens. Matter.* **2008**, *403*, 2193.
- Wang, Q.; Wei, X.; Dai, J.; Jiang, J.; Huo, X. *Mater. Sci. Semicond. Process.* **2014**, *21*, 111.
- Kim, Y.; Jeong, J. H.; Kang, M. *Inorg. Chim. Acta* **2011**, *365*, 400.